Computational Modeling of Temperature, Flow, and Crystallization of Mold Slag During Double Hot Thermocouple Technique Experiments

LEJUN ZHOU, WANLIN WANG, RUI LIU, and BRIAN G. THOMAS

A three-dimensional finite-difference model has been developed to study heat transfer, fluid flow, and isothermal crystallization of mold slag during double hot thermocouple technique (DHTT) experiments. During the preheating stage, temperature in the middle of the mold slag sample was found to be significantly [~350 K (~77 °C)] lower than near the two thermocouples. During the quenching stage, the mold slag temperature decreases with the cooled thermocouple. The temperature across the mold slag achieves a steady, nonlinear temperature profile during the holding stage; the insulating effect of the crystallizing layer in the middle of the slag sample causes the high temperature region to become hotter, while the lower temperature mold slag becomes cooler. Fluid flow is driven by Marangoni forces along the mold slag surface from the hotter region to the cooler region, and then recirculates back through the interior. Slag velocities reach 7 mm/s. Crystallization is predicted to start in the middle of the slag sample first and then grows toward both thermocouples, which matches well with observations of the DHTT experiment.

DOI: 10.1007/s11663-013-9864-2

I. INTRODUCTION

MOLD powder is widely used in modern continuous casting of steel, where it melts to form a liquid flux layer above the molten steel and infiltrates into the mold/shell channel. Mold flux functions are (1) to protect the steel from oxidation, (2) to insulate the steel and avoid meniscus freezing, (3) to absorb inclusions, (4) to lubricate the shell from sticking to the mold, and (5) to moderate the heat transfer in the mold. The crystallization of mold flux is regarded as one of the most important properties of mold flux because it greatly influences both heat transfer and lubrication.[1,2] Therefore, it is important to understand the crystallization behavior of mold slag.

It is difficult to observe slag behavior directly in the mold due to the high temperature production environment that makes visualization and measurement difficult. Furthermore, the mold adds complications involving powder melting, mold oscillation, transient fluid flow, complicated chemical reactions with the steel and atmosphere, and other phenomena. Thus, several different laboratory technologies have been developed to study the fundamental crystallization behavior of mold flux, including the double hot thermocouple technique (DHTT) and the single hot thermocouple technique (SHTT). The DHTT and SHTT were first developed by Kashiwaya *et al.*[3,4] for *in situ* observation of mold flux crystallization and are favored by many other researchers due to easy visualization as well as high heating and cooling rates.[5–10] However, only the temperature of the mold slag adhering to the thermocouples can be measured, making important effects on crystallization, such as spatial variations in temperature and fluid flow inside the mold slag sample, difficult to quantify. Moreover, fluid flow in the small, lump-shaped DHTT sample is dominated by natural convection and surface effects driven by Marangoni forces. This is very different from the real process, where the mold slag is shaped in the form of a large, thin sheet that is squeezed in the gap between an oscillating mold and a moving steel shell. Thus, it is problematic to apply the experimental results directly to the real casting process.

Fortunately, computer modeling offers a powerful tool to investigate these effects. Such models can be used to develop more fundamental property data. After the model simulation can accurately model the laboratory DHTT experiment, the validated model with the fundamental properties can be applied to simulate slag behavior in the gap of the real commercial casting processes.

This paper takes an initial step toward this goal by developing a numerical model of heat transfer, fluid flow, and mold slag crystallization using the commercial computational fluid dynamics (CFD) package Fluent[11] and applying it to match observations and measurements

---

LEJUN ZHOU, Graduate Student, is with the School of Metallurgical Science and Engineering, Central South University, Changsha 410083, People's Republic of China, and also Visiting Scholar with the Department of Mechanical Science and Engineering, University of Illinois at Urbana-Champaign, 1206 W. Green Street, Urbana, IL 61801. WANLIN WANG, Professor, is with the School of Metallurgical Science and Engineering, Central South University. Contact e-mail: wanlin.wang@gmail.com RUI LIU, Graduate Student, and BRIAN G. THOMAS, C.J. Gauthier Professor, are with the Department of Mechanical Science and Engineering, University of Illinois at Urbana-Champaign.

Manuscript submitted December 3, 2012.

of the DHTT experiment. The results provide better understanding of the interaction among temperature variations in the slag sample, the movement of crystals driven by Marangoni flow and natural convection, and the crystallization of mold slag.

II. SHTT AND DHTT EXPERIMENTS

In the SHTT experiment, pictured in Figures 1(a) and (b), a small (about 0.05 g) sample of mold flux powder is mounted in a thermocouple shaped into a half loop, heated to a desired preheat temperature, and held for several minutes. After the powder melts to form a transparent molten slag, the thermocouple is quenched at a prescribed rate, to a constant holding temperature, while crystallization of the slag is visually observed through a microscope and recorded by a connected CCD onto a DVD. The DHTT experiment, shown in Figures 1(a) and (c), uses two B-type thermocouples to suspend the molten slag sample in order to provide a controlled, time-dependent temperature gradient across the sample by independent cooling of the two thermocouples. The experiments were conducted in air, with resistance heating provided by DC current through the thermocouple wires, using a silicon-controlled rectifier (SCR) controller to maintain the prescribed temperature histories within ±275 K (±2 °C).

SHTT and DHTT experiments were performed on a typical slag used for continuous casting of low-carbon steel, owing to the slow, easily observed crystallization process for this composition. The composition of the premelted mold flux is shown in Table I. The samples were prepared by melting a mixture of seven chemically pure minerals in an induction furnace at 1773 K (1500 °C) for 5 minutes to homogenize its chemical composition. The carbon found in commercial mold powders to slow the melting rate is not added to the samples here in order to simulate the composition of the melted flux found in the protected slag layer in the gap between the mold and shell of the real process. Next, the slag was poured onto a cool steel plate to quench and then crushed and ground to make sample powders for the DHTT and SHTT experiments. Further details on these experiments applied to slags for low- and medium-carbon steel can be found elsewhere.[12]

As shown in Figure 1(c), the slag sample in the DHTT is mounted between two thermocouples (CH-1 and CH-2) and subjected to a temperature gradient history chosen to roughly approximate the thermal conditions expected in the continuous casting mold.[7,12]

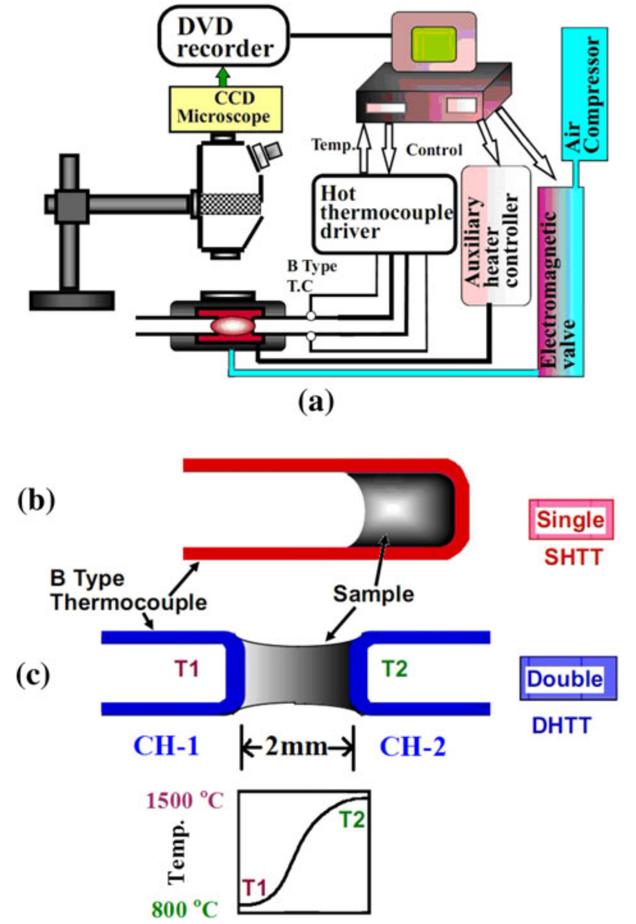

Fig. 1—Schematic of the SHTT and DHTT experiments.[3]

The recorded (and simulated) temperature histories of the DHTT experiment are shown in Figure 2. Simulation time starts near the end of preheating ($t = 0$ second) and was found by simply subtracting 267 seconds from the "unadjusted" time measured from the start of the experiment, as shown in Figure 2. Only simulation time is used for the rest of the paper. The simulation of this experiment was divided into three stages: stage 1 preheating (from 0 to 10 seconds), stage 2 quenching (from 10 to 35 seconds), and stage 3 holding (from 35 to 643 seconds), according to different thermal boundary conditions.

Typical pictures of the DHTT experiment showing evolution of the crystalline layer are given in Figure 3. The crystalline layer first appears in the middle of the mold slag at 154 seconds (53 seconds after quenching) and grows toward both thermocouples. In addition, fluid flow can be observed in the original video recordings of both SHTT and DHTT experiments, as the molten mold slag is seen to transport some small crystals from the central region of the liquid slag sample toward the hot thermocouple. These observations are explained by the numerical model of the crystallization process, which is presented in the next section.

Photographs of the SHTT experiment, Figure 4, track the growth of crystallized area fraction. Note that the region at the far left is discolored due to refraction, so its area is not counted. Time–temperature–transformation (TTT) diagrams were constructed from the recorded temperature and time and fraction transformed.

III. MODEL DESCRIPTION

A model of heat transfer, fluid flow, and crystallization of the DHTT experiment has been developed for the geometry shown in Figure 5. The three-dimensional

Table I. Mineral Percentage of the Premelted Mold Fluxes[12]

	CaO	SiO_2	Al_2O_3	MgO	CaF_2	Na_2O	Li_2O
Mass percentage	25.1	41.5	7.1	2.0	12.1	9.2	0.5
Mole fraction	0.28	0.43	0.04	0.03	0.10	0.09	0.01

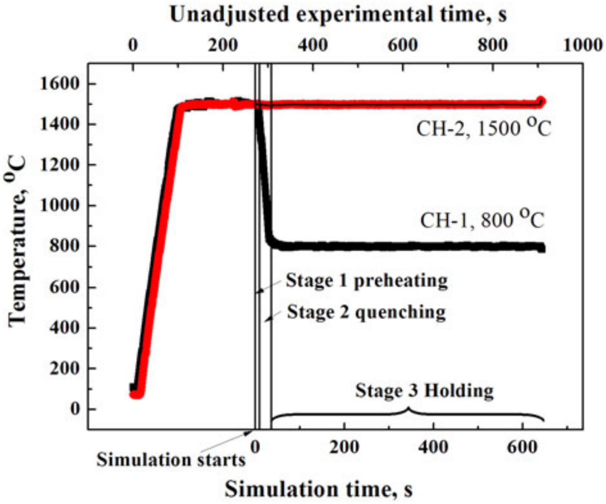

Fig. 2—Temperature history of DHTT experiment.

simulation domain of the 0.05-g mold slag sample is based on the measured shape of the actual slag sample from photographs, with angles shown in Figure A2 (Appendix). These angles are based on the sagging shape of the sample which is governed by the combined forces of surface tension and gravity, as presented in the Appendix. This domain does not include the thermocouples, which act as fixed-temperature, non-slip boundaries.

A. *Governing Equations*

The transient conservation equations of mass, momentum, and energy[13] are solved in three dimensions for velocity and temperature distribution in the mold slag. The mass conservation or "continuity" equation is given by

$$\nabla \cdot (\vec{\mathbf{v}}) = 0 \qquad [1]$$

where $\mathbf{v}$ is the fluid velocity vector.

The equation for momentum conservation of an incompressible Newtonian fluid is given as follows, including the buoyancy body force to include the influence of natural convection.

$$\rho_0\left(\frac{\partial \vec{\mathbf{v}}}{\partial t} + \vec{\mathbf{v}}\nabla\vec{\mathbf{v}}\right) = -\nabla p + \mu\nabla\nabla\vec{\mathbf{v}} + \rho\mathbf{g} \qquad [2]$$

where p is the static pressure, μ is viscosity, and $\mathbf{g}$ is the gravitational acceleration. Gravity acts in the Z direction, as shown in Figure 5, and the standard Boussinesq approximation is applied, which accurately incorporates the effect of temperature-dependent density ρ on buoyancy-driven flow in incompressible fluids for small density changes[11]:

$$\rho = \rho_0(1 - \beta\Delta T) \qquad [3]$$

where ρ_0 is the density at a reference temperature (298 K) and β is the thermal expansion coefficient of the mold slag (K^{-1}).

The energy conservation equation, including the effects of transient conduction, advection, diffusion, and heat sources, is

$$\rho C_p \frac{\partial T}{\partial t} + \rho C_p \vec{\mathbf{v}}\nabla T = \nabla(k_{\text{eff}}\nabla T) + S_h \qquad [4]$$

where k_{eff} is the effective conductivity (including conduction and radiation). The energy source term S_h was added to consider the latent heat of mold slag crystallization in those cells where phase transition (crystallization) occurs.

$$S_h = \rho\frac{dH_{\text{CLH}}}{dt} = \rho\frac{dH_{\text{CLH}}}{df}\frac{df}{dt} \qquad [5]$$

where H_{CLH} is the latent heat of crystallization of the mold slag and f is the crystallized phase fraction.

B. *Isothermal Crystallization Model*

A model of isothermal crystallization was developed for the mold slag by defining and tracking the crystallized phase fraction f of the mold slag. The function is based on the temperature-dependent incubation time obtained from single hot thermocouple experiments.[12] At times shorter than the incubation time, $f = 0$, indicating that the slag is totally liquid; otherwise, $f = 1$, indicating that the slag has started to crystallize.

The theoretical incubation time, τ (seconds), can be found by evaluation of the Johnson–Mehl–Avrami (JMA) model,[14,15] fitted to the SHTT data.

$$f = 1 - \exp\{-[k(t-\tau)]^n\} \qquad [6]$$

where f is the volume fraction of crystals, t is crystallization time (seconds), k is the effective crystallization rate constant including nucleation and growth (s^{-1}), and n is the dimensionless Avrami exponent that is associated with the nucleation and growth mechanism.

Due to the video resolution limitations, it is impossible to observe initiation of the first crystals in the SHTT experiment, which defines the theoretic incubation time. Instead, evaluating Eq. [6] at 5 pct crystalline fraction and rearranging gives

$$\ln\ln\left(\frac{1}{1-f_{0.05}}\right) = n\ln k + n\ln(\tau_{0.05} - \tau) \qquad [7]$$

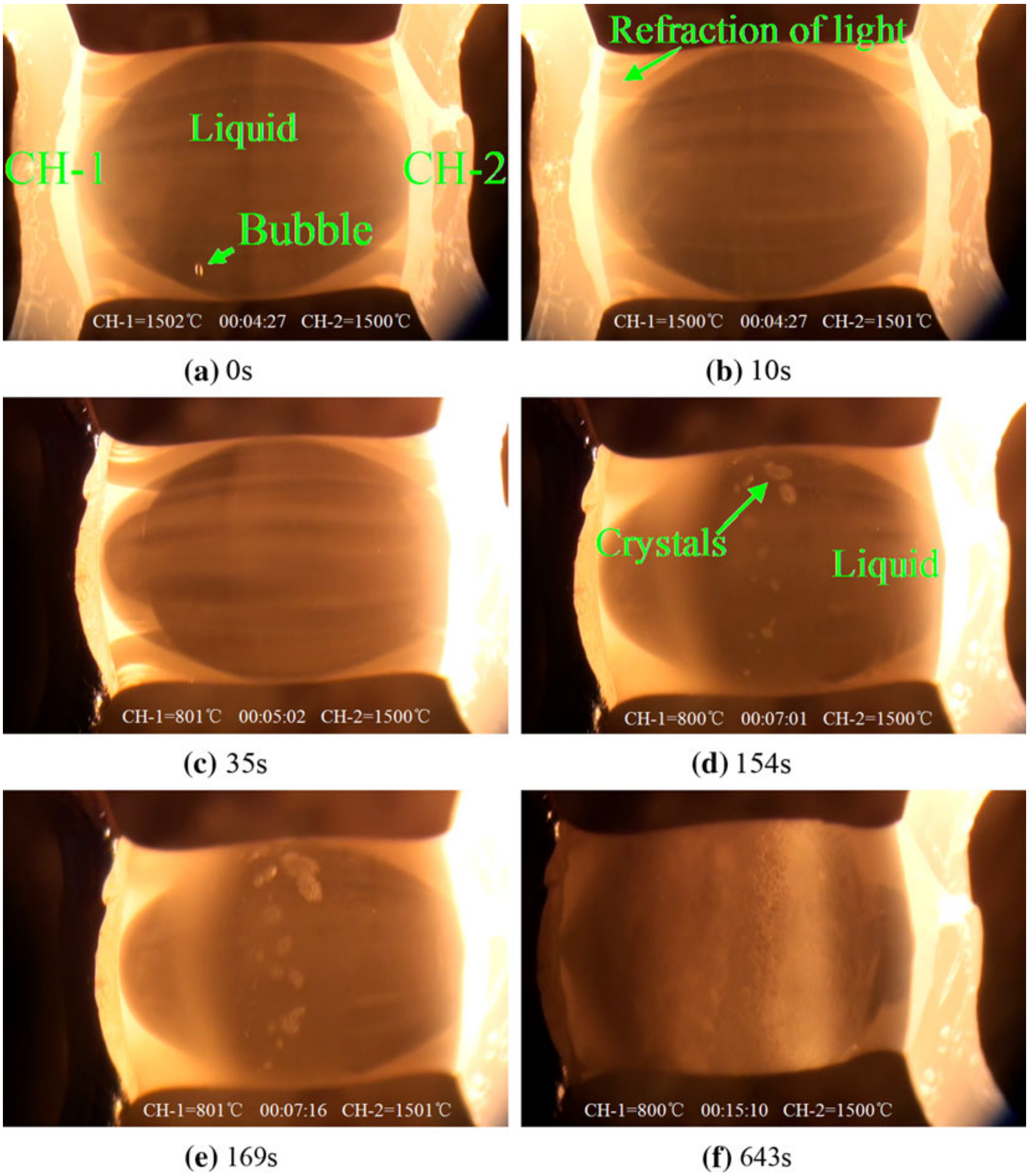

(a) 0s **(b)** 10s

(c) 35s **(d)** 154s

(e) 169s **(f)** 643s

Fig. 3—Evolution of crystalline layer in DHTT experiment.[12] Note: Time labels are simulation time.

where $f_{0.05}$ is the crystalline fraction = 0.05; $\tau_{0.05}$ is the corresponding time when the crystalline fraction is 5 pct.

The values of parameters n and k at different temperatures were calculated by plotting $\ln\ln(1/(1-f+f_{0.05}))$ *vs* $\ln(t-\tau_{0.05})$ as shown in Figure 6. Fitted results are listed in Table II. Then, using Eq. [7], the theoretic incubation time τ was estimated and is given in Table III.

The incubation time, τ (seconds), is given as a function of temperature (K) in Eq. [8] and plotted in Figure 7.

$$\tau = f(T) = A_0 + A_1T + A_2T^2 + A_3T^3 + A_4T^4 + A_5T^5 \quad [8]$$

where A_0 = 1.47, A_1 = 379.58093, A_2 = −1.15396779, A_3 = 0.00131489225, A_4 = -6.65604E^{-7}, and A_5 = 1.2635228E^{-10}.

C. *Boundary Conditions*

The DHTT slag sample is suspended between two thermocouples, CH-1 and CH-2. During the preheating stage 1, both thermocouples were held at a fixed temperature of 1773 K (1500 °C). Energy comes from the two thermocouples, travels across through the mold slag, and is released into the air through radiation. During the quenching stage 2, the CH-1 was cooled down from 1773 K to 1073 K (1500 °C to 800 °C) at a cooling rate of 30 K/s, while CH-2 was maintained at

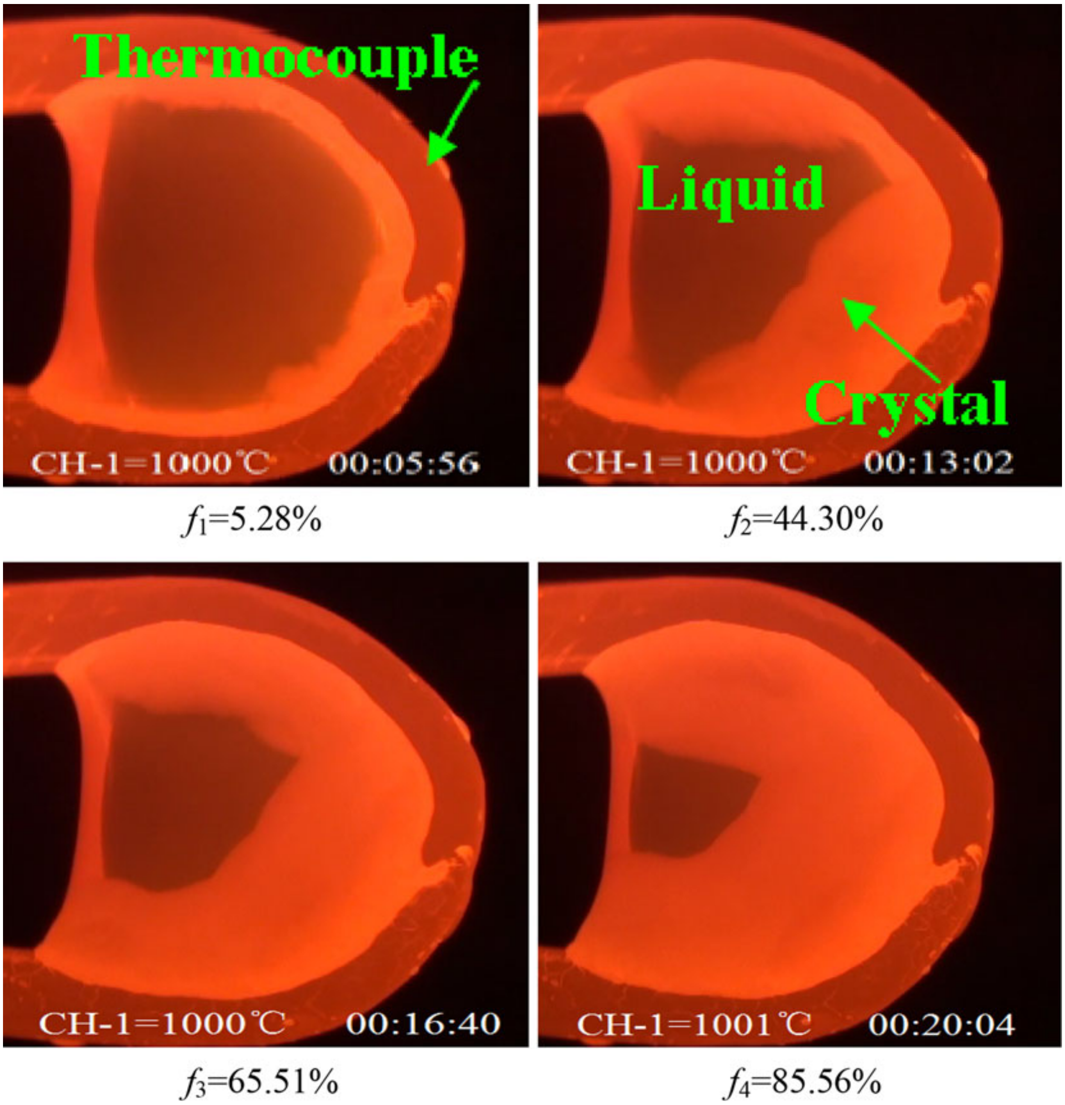

f_1=5.28%

f_2=44.30%

f_3=65.51%

f_4=85.56%

Fig. 4—Variation of volume fraction of crystallites in SHTT test.

1773 K (1500 °C). The commercial mold can produce very high cooling rates,[16] but 30 K/s was the fastest possible with this apparatus. During the holding stage 3, the CH-1 and CH-2 were held at temperature of 1073 K and 1773 K (800 °C and 1500 °C), respectively. The remaining four surfaces of the slag sample are subjected to radiation cooling during all stages using an effective gray-body external emissivity. Natural convection heat removal from the sample surfaces was ignored here since it is small compared with radiation loss.

Shear-stress wall boundary conditions are imposed on the top, bottom, front, and rear surfaces in this model to incorporate the Marangoni forces caused by the temperature-dependent surface tension of the mold slag.[13] This shear stress is defined by

$$\mu \frac{\partial v_r}{\partial n} = \frac{d\gamma}{dT} \frac{\partial T}{\partial r} \qquad [9]$$

where $\frac{d\gamma}{dT}$ is the surface tension gradient with respect to temperature, $\frac{\partial T}{\partial r}$ is the temperature gradient in direction r along the surface, and n is in the direction perpendicular to the surface. The surfaces of the flow domain at the thermocouples are non-slip walls.

D. *Material Properties*

The thermal and fluid properties of the mold slag used in this computation are listed in Table IV. Calculation of the surface tension gradient is discussed in the Appendix.

E. *Numerical Solution Details*

The model equations were solved using the commercial CFD software ANSYS Fluent (version 13.0, ANSYS Inc.)[11] with the Gambit preprocessor. The control-volume technique was used to discretize the governing equations. The domain was divided into 84,916 hexahedral volume elements. The discretization schemes used in this numerical calculation were quadratic upwind interpolation of convective kinematics (QUICK) for momentum and energy equations,

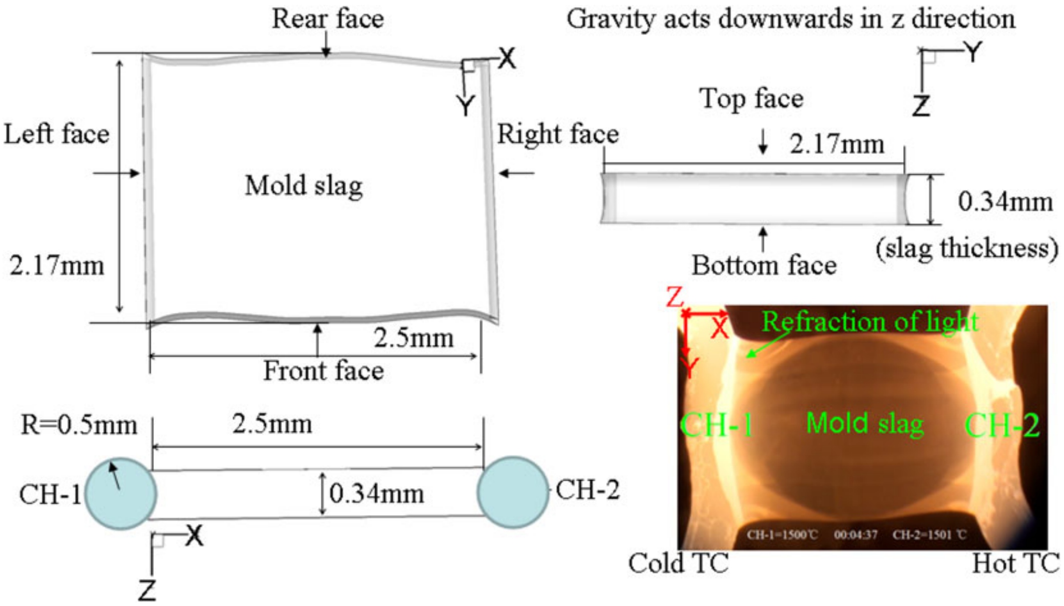

Fig. 5—Model simulation domain for DHTT experiment.

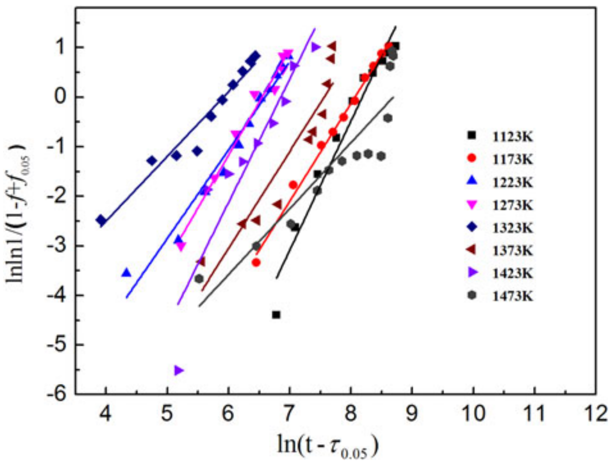

Fig. 6—The relation of crystalline fraction evolution with time.

Table II. Values of n and k (Eq. [7]) at Different Temperatures

Temperature [K (°C)]	n	ln(k)
1123 (850)	2.62	−8.18
1173 (900)	1.92	−7.55
1223 (950)	1.76	−6.69
1273 (1000)	2.13	−6.55
1323 (1050)	1.31	−5.88
1373 (1100)	1.96	−7.54
1427 (1154)	1.63	−7.48
1473 (1200)	1.33	−8.69

body force weighted for pressure, and semi-implicit method for pressure-linked equations (SIMPLE) for pressure–velocity coupling.[11] The crystallization model is incorporated using a user-defined function (UDF) memory variable to indicate the mold slag phase fraction of crystal or liquid/glass. In stage 1, the time step size was set as 0.001 second, and the number of time steps was 10 in the first 0.01 second; then, through 0.02 to 0.1 seconds, the time step was set as 0.01 second, and the number of time steps was 9; and through 0.2 to 1 seconds, the time step was set as 0.1 second, and the number of time steps was also 9. After 1 second, the time step was set as 1 second for the rest of the simulation. The maximum number of iterations was set as 20 per time step in the entire calculation. The convergence criterion was 10^{-6}, which means that the scaled residual of the final solution is reduced to 10^{-6} of the initial residual.

F. *Model Validation*

The computational model was first validated by comparing its predictions with analytical solutions to simplified test problems, chosen to have similar conditions and dimensions to the current mold slag model. Furthermore, the same mesh refinement, numerical methodology, and convergence criteria are used in the computational modeling of the test problem and of the DHTT experiment. In this work, the temperature profile during transient one-dimensional heat conduction with solidification of a semi-infinite plate for "metal-control"[17] was matched within 0.2 pct error at 1 second using a mesh of 61,400 computational cells with 89 cells through the solidified thickness. In this test problem, which has no kinetic effects in latent heat evolution, both solutions predict that a 1-mm slag layer takes less than 1 second to solidify. Further validation of the computational model was accomplished by comparison with experimental observations, which are described with the results in the next sections.

Table III. Theoretic Incubation Times (Eq. [8]) at Different Temperatures

Temperature [K (°C)]	1123 (850)	1173 (900)	1223 (950)	1273 (1000)	1323 (1050)	1373 (1100)	1427 (1154)	1473 (1200)
Incubation time (s)	246	155	105	172	190	233	310	442

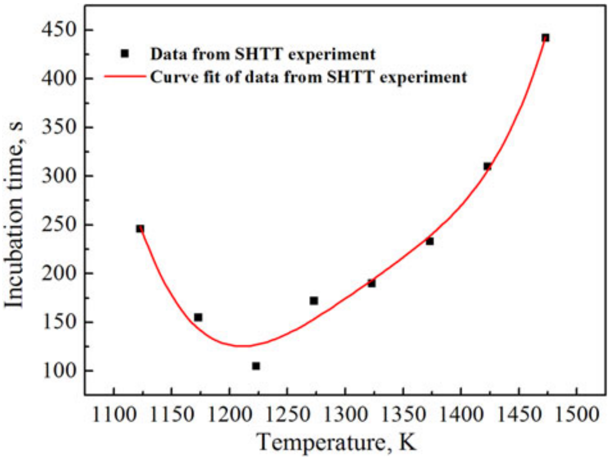

Fig. 7—The relation of incubation time with temperature.

Table IV. Thermal and Fluid Properties of Mold Slag

Specific Heat, C_p (J/kg/K)	$1100 + 0.063T$ (K) $-3.5 \times 10^{-7}/T^2$[27]
Latent heat of crystallization, H_{CLH} (J/kg)	6.1×10^5[27]
Effective thermal conductivity, k_{eff} (W/m/K)	Liquid: 3[20,28] Crystalline: 1.7
Emissivity, σ	0.8[28–30]
Viscosity, μ (kg/m/s)	$-8.194 + 11989.17/T$[31]
Density, ρ (kg/m^3)	$3021 - 0.33T$[25,32,33]
Thermal expansion coefficient, β (K^{-1})	1.1×10^{-4}[25,32,33]
Surface tension gradient, $d\gamma/dT$ (N/m/K)	-0.00012[26,34]

IV. TEMPERATURE AND FLOW: RESULTS AND DISCUSSION

The numerical model predictions of the DHTT experiment are presented for the preheating stage and then for quenching and holding stages.

A. *Preheating Stage 1: Temperature*

During the preheating stage 1, the temperature of both thermocouples was kept constant at 1773 K (1500 °C) from 0 to 10 seconds. Figure 8 shows the steady-state temperature distribution at 10 seconds, at the end of stage 1. The red surface temperature contours near the thermocouples represent the higher temperature region, while the blue central region is at a lower temperature. The middle of the mold slag is slightly cooler due to the heat lost *via* radiation from the sample surfaces. This matches the snapshot of the DHTT experiment in the lower right frame, where the mold slag middle region is darker, indicating a lower temperature.

Temperature profiles at different times are shown in Figure 9(a), taken along the central line through the domain in the X direction, as indicated in Figure 9(b). The lowest temperature is 1407.2 K at the sample center. The mold slag middle cooled down very fast, reaching steady state within 0.1 second. The high cooling rate is due to the very thin (0.34 mm) mold slag layer in the DHTT sample. This fast response rate insures that the slag temperature distribution remains constant during the rest of stage 1 and during stage 3.

The non-uniform temperature distribution, with 350 K (77 °C) variations, is very noteworthy. This result means that the slag samples in the DHTT and SHTT test experience significant temperature gradients and cannot be assumed to have isothermal behavior. During "isothermal" crystallization experiments, the mold slag may crystallize first near the sample center, at the lower temperature there, in spite of the lack of the thermocouple as a nucleation site. The correct extraction of TTT curves from these experiments is complicated by this non-isothermal behavior. Thus, models such as that of the current work are needed to help with this analysis.

B. *Preheating Stage 1: Fluid Flow*

The non-uniform temperature distribution during preheating induces fluid flow *via* two mechanisms. Marangoni flow is generated by the difference of surface tension along the slag sample surface and natural convection inside the mold slag results from the temperature differences in the bulk. Figure 10 shows the resulting velocity vector distribution at 10 seconds in stage 1. Figures 10(b), (c), and (d) show views in the $X_1 - X_2$, $Y_1 - Y_2$, and $Z_1 - Z_2$ sections, respectively, as indicated in the 3-D view in Figure 10(a). The arrows on the velocity vectors indicate the direction of flow. Flow along the sample surfaces is driven from the hotter region near both thermocouples toward the cooler region in the middle (Figure 10(a)), and then flow recirculates back through the interior from the cooler region to the hotter region of the mold slag, as shown in Figure 10(b). This flow is driven mainly by Marangoni forces, as the cooler, high surface tension middle pulls fluid along the surface from the hotter, low surface tension thermocouple region. Return flow through the interior is driven by mass conservation. Natural convection is relatively unimportant because there is very little asymmetric flow associated with the Z (gravity) direction. Velocity magnitude increases toward the higher temperature regions near both thermocouples due to the lower viscosity caused by the higher temperatures there.

Figure 11 shows detailed velocity magnitude profiles along the X axis direction at the top face, center plane, and bottom faces (Figure 9(b)) at 10 seconds. The curves are "M" shaped. Velocity is zero at the non-slip

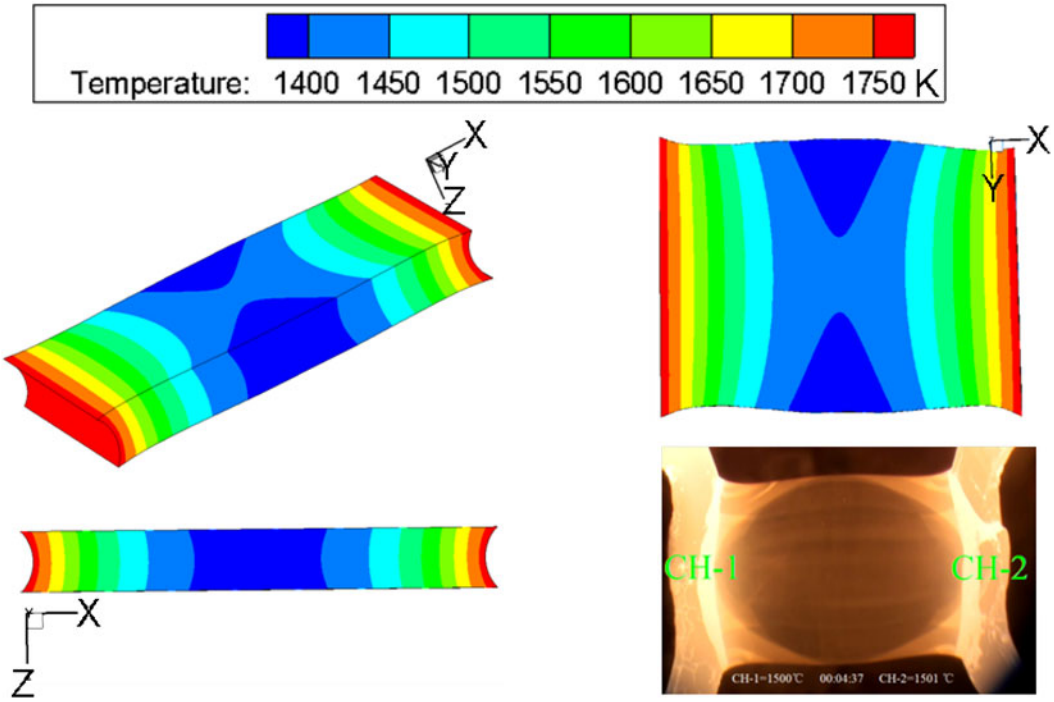

Fig. 8—Temperature contours at time of 10 s in stage 1.

interfaces with the thermocouples, and at the center, due to symmetry. Velocity along the top and bottom faces is the same, indicating symmetry of temperature and fluid flow in the central plane. The maximum velocity reaches 7 mm/s along the surface near the thermocouples. This corresponds to a Reynold's number $vL\rho/\mu$ (based on L = sample thickness) of 0.054, so the laminar flow assumption is appropriate. Velocity along the surface is higher than the interior region, including the center plane.

The variation of the centerline velocity profile with time is shown in Figure 12. The highest velocity of 4 mm/s develops after only 0.5 second. As time increases from 0 second (uniform temperature), the temperature in the middle of the interior drops quickly, generating temperature gradients which enhance the buoyancy and Marangoni effects, and so the velocity increases.

This fluid flow may break up central crystalline aggregation and transport crystals into higher temperature regions. The movement of crystals toward the thermocouples has been observed both by Cramb[7] as shown in Figure 13(a) and in the present work (Figure 13(b)). Inferring the flow direction at different depths from observation of the moving crystals is difficult in a transparent medium. Most crystals form in the cool central region of the sample and are observed to move toward the hot thermocouple(s). The flow model results suggest that this movement is occurring through the sample interior. It seems that the return flow taking place in the thin surface layer is difficult to observe, although the strong velocity gradients can be inferred from the observed breakup of large crystalline aggregations as they move.

C. *Quenching Stage 2*

During the quenching stage 2, from 11 to 35 seconds, the CH-1 thermocouple cools from 1773 K to 1073 K (1500 °C to 800 °C) at a cooling rate of 30 K/s, while the hot thermocouple CH-2 is held at 1773 K (1500 °C). During the holding stage 3, after 36 seconds, the temperatures are kept constant. The temperature distribution at the end of quenching, 35 seconds, is shown in Figures 14(a) through (c). Temperature is observed to increase from left to right, which is consistent with the increasing brightness toward the right, seen in the real experiment snapshot in Figure 14(d).

Figure 15 quantifies the temperature profile along the central X-direction line (Figure 9(b)) with time during quenching stage 2. The temperature near the left (CH-1) naturally drops much faster than near the right (CH-2). After 35 seconds, the temperature profile remains constant. This temperature distribution thus defines the isothermal crystallization temperature during stage 3.

The time variation of temperature and cooling rates at different distances away from CH-1 in the mold slag is shown in Figures 16 and 17, respectively. The starting temperatures at 10 seconds vary according to Figure 15. Thus, temperatures drop at different rates with the quenching of CH-1 over the next 25 seconds. Subsequently, temperatures become constant almost immediately due to the small thickness of the mold slag sample, as discussed previously.

Figure 17 shows that the mold slag next to CH-1 has the highest cooling rate of 30 K/s. The cooling rate decreases with distance away from CH-1. A similar distribution is expected across the mold slag layers in the interfacial gap between the mold and the solidifying steel

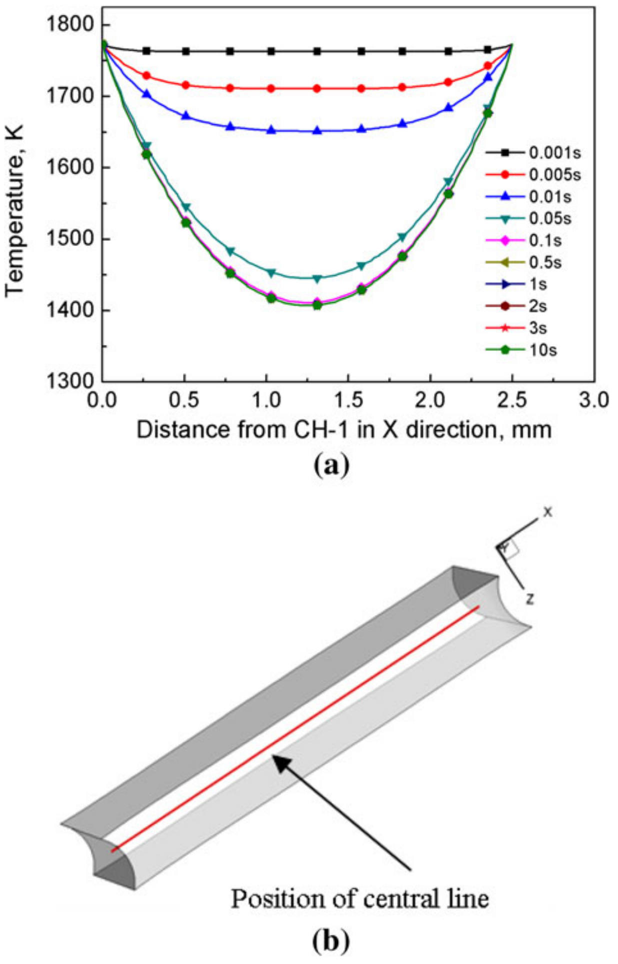

Fig. 9—Temperature distribution along the central line at different times in stage 1.

shell of a continuous caster, where the slag near the water-cooled mold wall has the highest cooling rate, while near the shell, it has the lowest.

The time–temperature histories determine whether the molten slag transforms into a glassy phase or crystals. Figure 18 shows the isothermal TTT diagram for the mold slag of this work. The critical cooling rate is 5.24 K/s ($\frac{1773\ \mathrm{K}\ (1500\ ^\circ\mathrm{C})\ \mathrm{to}\ 1223\ \mathrm{K}\ (950\ ^\circ\mathrm{C})}{105\ \mathrm{seconds}}$). When the local cooling rate is less than this critical cooling rate, crystals can form, with size and morphology depending on the cooling history. Otherwise, the supercooled liquid may simply form glass. In this work, most of the slag is initially glassy, owing to the cooling rates exceeding this critical value in most of the sample.

The initial glassy layer may later transform to crystals, or "devitrify," if subsequently the temperature is maintained hot enough for a time period long enough to exceed the isothermal incubation time. This eventually led to complete crystallization in the current sample. This behavior is also commonly experienced by slag near the mold wall in the steel continuous caster.[18] High local contact resistance between the mold wall and slag combined with very slow movement of the solid portion of the solid slag explains why the mold slag layer next to the mold wall is usually crystalline.[16,19]

The stable flow pattern in Figure 10 generally slows during quenching. The evolution of the velocity profile across the mold slag sample length with time during this stage is given in Figure 19. The decrease in temperature near CH-1 causes significant increase in viscosity, which decreases velocity in the cold half of the sample. Velocity in the hot region near CH-2 increases slightly during this time period.

D. *Holding Stage 3*

During the isothermal holding stage (after 35 seconds), crystallization occurs in the mold slag sample, starting in the center region. While the temperature history controls the evolution of the crystalline layer, the crystalline layer in turn affects the temperature distribution. Figure 20 shows the nonlinear temperature distribution along the central line in X axis at 35 and 470 seconds during holding. The higher temperature region near CH-2 gets slightly hotter during holding. At the same time, the lower temperature region close to CH-2 gets slightly cooler. This temperature variation, that reaches maximum 40 K (−233 °C), is included in Figure 20 and can be explained by the change of phase of the mold slag. The effective thermal conductivity of the mold slag decreases when it crystallizes due to the formation of internal defects, such as pores, and the inhibition of radiative heat transfer, caused by the scattering from crystal defects and grain boundaries as found in previous studies.[20–22] Thus, the crystallized slag provides an insulating layer which reduces the heat flux transferring from the higher temperature region to the lower temperature region. The evolution of latent heat during crystallization further increases this effect. Although the effect is observed here to be relatively small, perhaps owing to the simplified treatment of radiation through the slag in the present model, the control of the mold slag crystallization is considered to be an effective method to control heat transfer and improve slab surface and interior quality in continuous casting.[21,23]

The fluid flow distribution during the holding stage 3 is shown in Figure 21, for the same four views as Figure 10. The flow behavior is similar in the high temperature region, but is suppressed in the half of the sample nearest the quenched CH-1. Molten slag is driven along the surface from the hotter region near CH-2 toward the cooler region and then returns back to the hotter region through the interior.

V. CRYSTALLIZATION MODEL PREDICTIONS

The model predictions of the evolving crystalline layer are shown in Figure 22(a), along with corresponding photos of DHTT experiments at similar times in Figure 22(b). In the first two frames of both the predictions and measurements, there are no crystals precipitated. A crystalline layer appears in the middle of the mold slag in the third frame. The positions of the

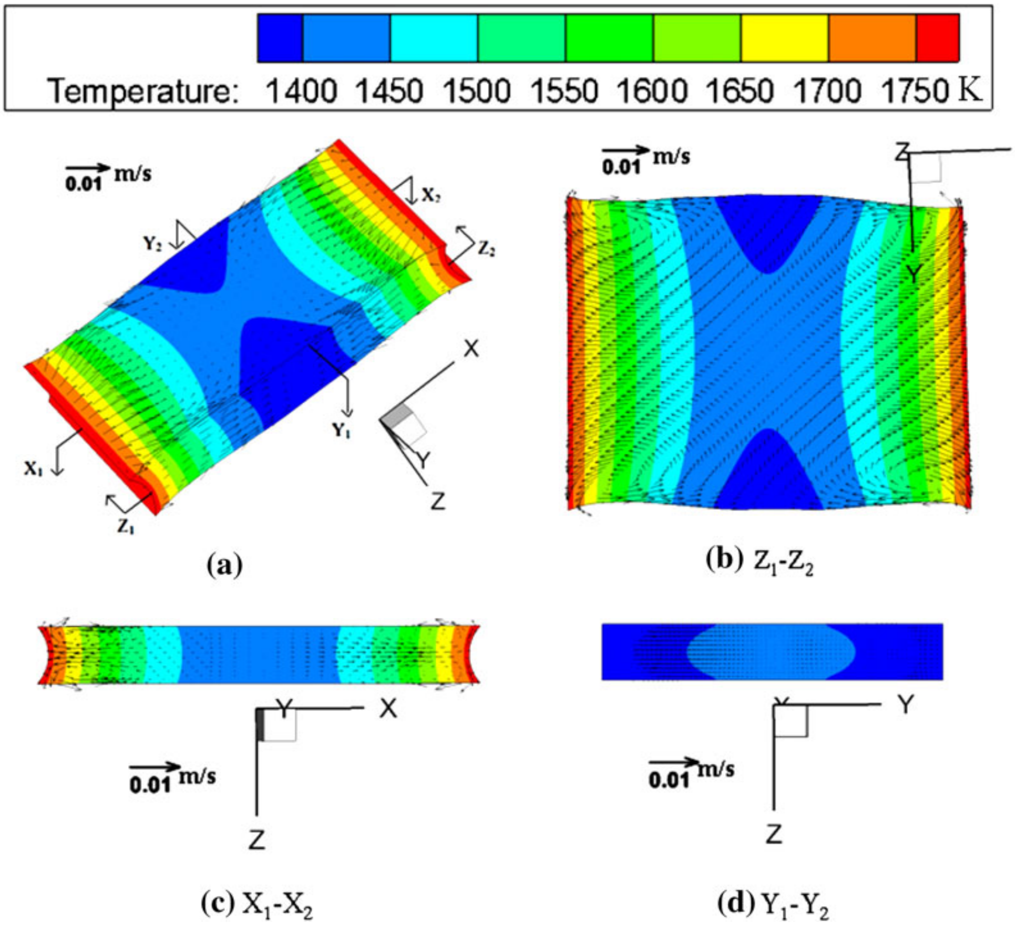

Fig. 10—Fluid flow at time of 10 s in stage 1.

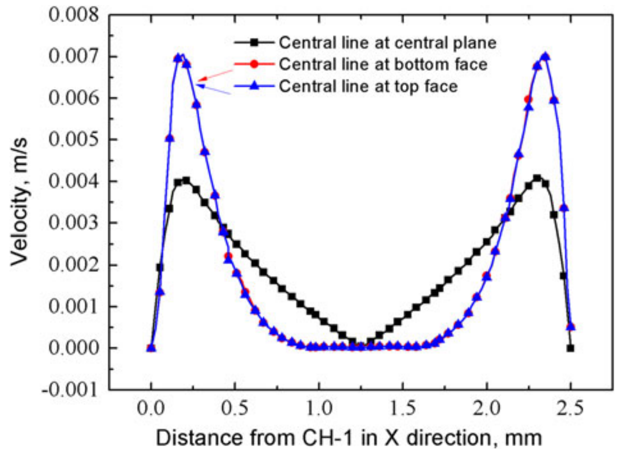

Fig. 11—Velocity magnitude at 10 s along centerline at top face, center plane, and bottom face.

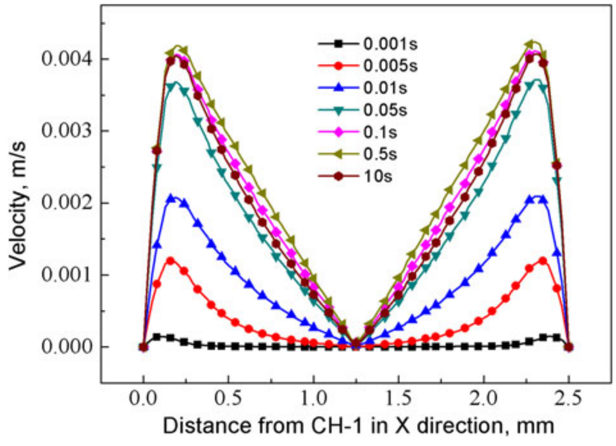

Fig. 12—Velocity magnitude along central line at central plane.

crystal layer in the third and fourth frames match well with the crystal precipitation observed in the experiment. However, small deviations arise with increasing time. The predicted growth of the crystalline layer is slower than the observations at later time (frames).

A likely explanation for this deviation is the difference between the idealized and actual SHTT and DHTT experiments. Applying the JMA model of incubation based on the SHTT data to the DHTT experiment assumes simple isothermal crystallization in both experiments and with no fluid flow. Actually, this work shows that non-uniform temperature gradients are significant and that fluid flow transports crystals after they form. A related complication is the associated differences in

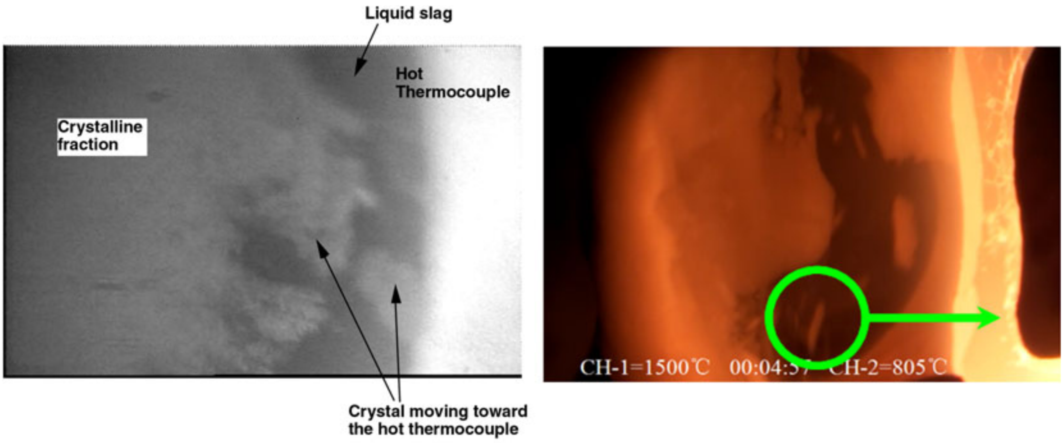

Observed by Prof. Cramb[7]

Observed in this work

Fig. 13—Crystals separate and move with flow in liquid mold slag.

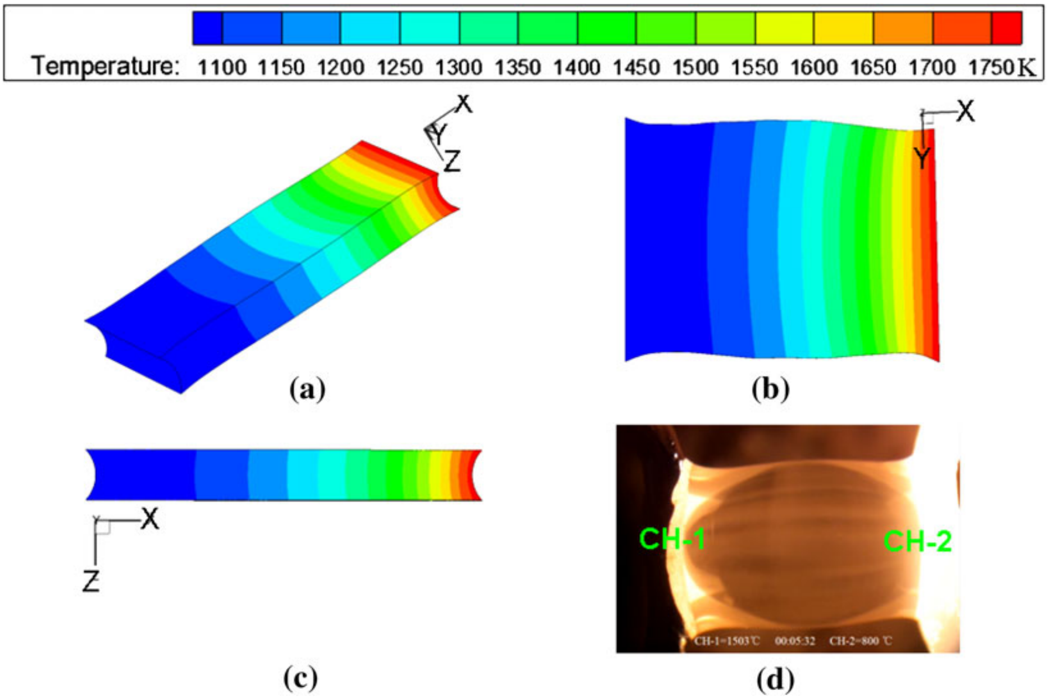

Fig. 14—Temperature contours at 35 s when TC-1 has cooled to 1073 K (800 °C).

heterogeneous nucleation between the two experiments. In the SHTT experiment, crystals often nucleate heterogeneously on the thermocouple wire and only sometimes initiate homogeneously in the middle of the mold slag. In the DHTT experiment, crystals always appear first in the middle of the slag sample, and the fluid flow tends to break and transport them, thus avoiding the need for homogenous nucleation. Therefore, the mold slag crystallizes faster in the DHTT experiment than expected. Future models should incorporate these effects to enable more accurate predictions.

Another error source is the difficulty of interpreting the discolored area fractions in the photographs as crystallized volume fractions. Also, the much longer time of the SHTT experiment likely allowed the composition of the slag in this experiment to change due to the volatilization of fluorides, *etc.*, which could slow the crystallization. Finally, humidity differences could have caused different rates of hydrogen pickup, which is known to greatly accelerate crystallization.[24] Considering these issues, the current model prediction of the onset of crystallization and trend of crystalline layer

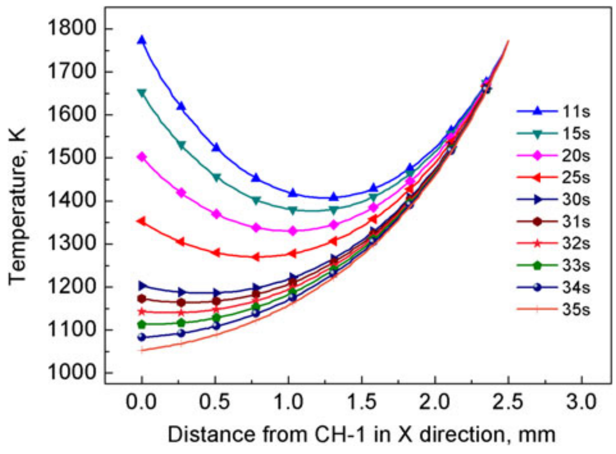

Fig. 15—Temperature distribution in *X* direction.

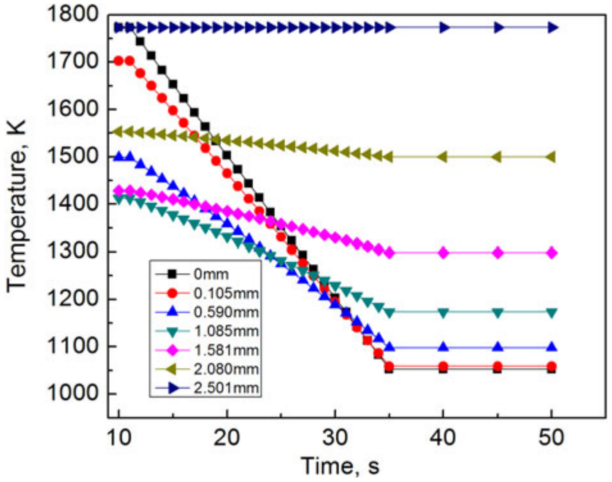

Fig. 16—Temperature variation with time at different distances from CH-1 along centerline between thermocouples.

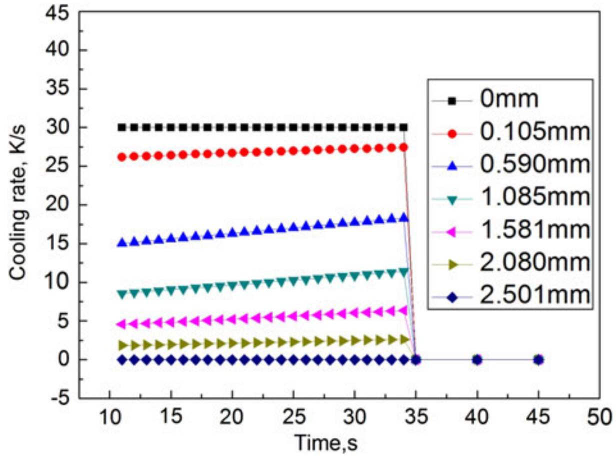

Fig. 17—Cooling rate variation with time and distance from CH-1 along centerline between thermocouples.

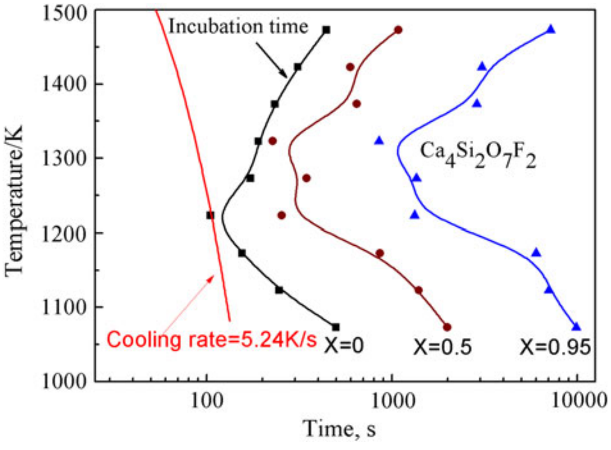

Fig. 18—TTT diagram of current mold slag.[12]

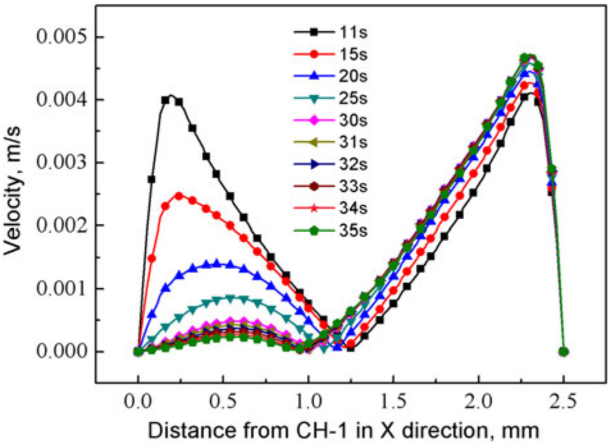

Fig. 19—Velocity magnitude along centerline of central plane during quenching stage 2.

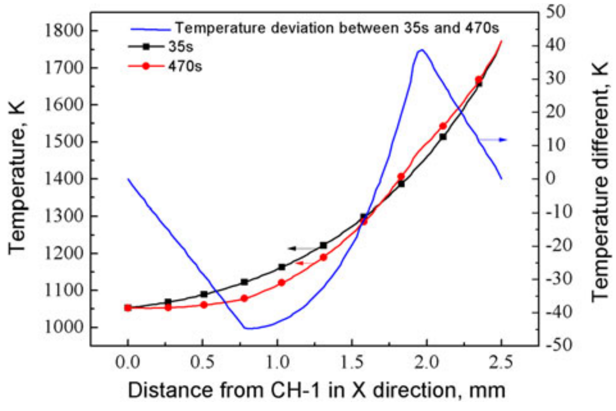

Fig. 20—Temperature and its variation along slag centerline during stage 3.

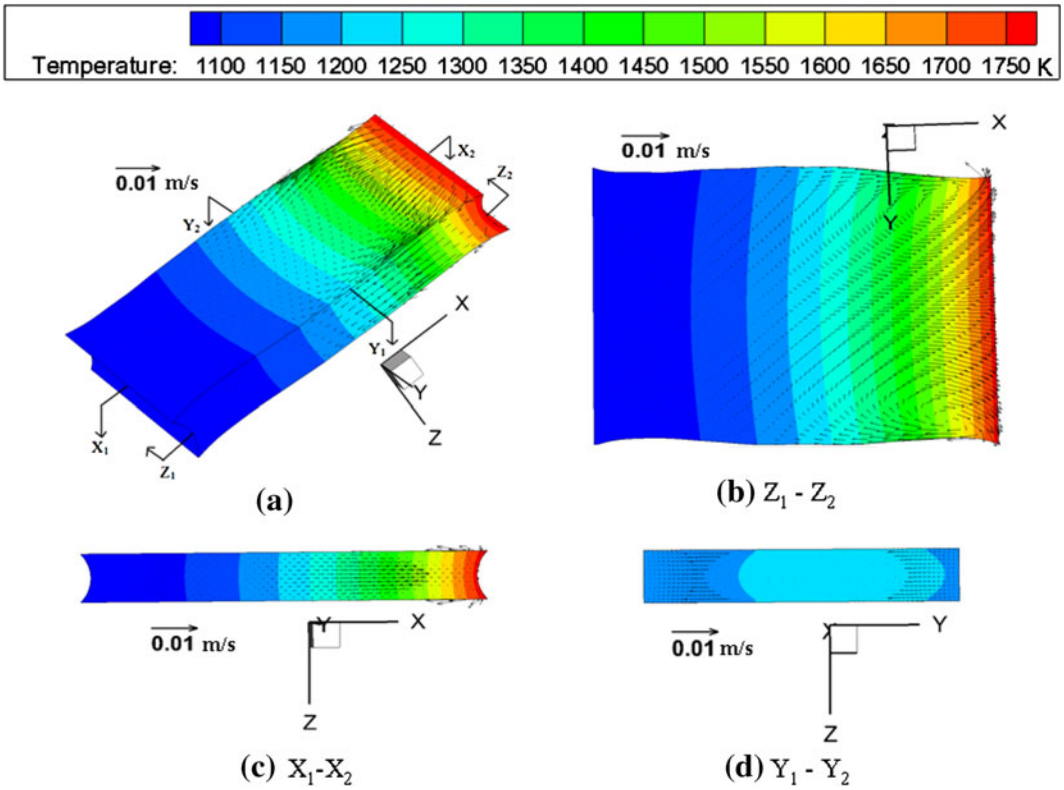

Fig. 21—Fluid flow distribution at 35 s end of quenching stage 2).

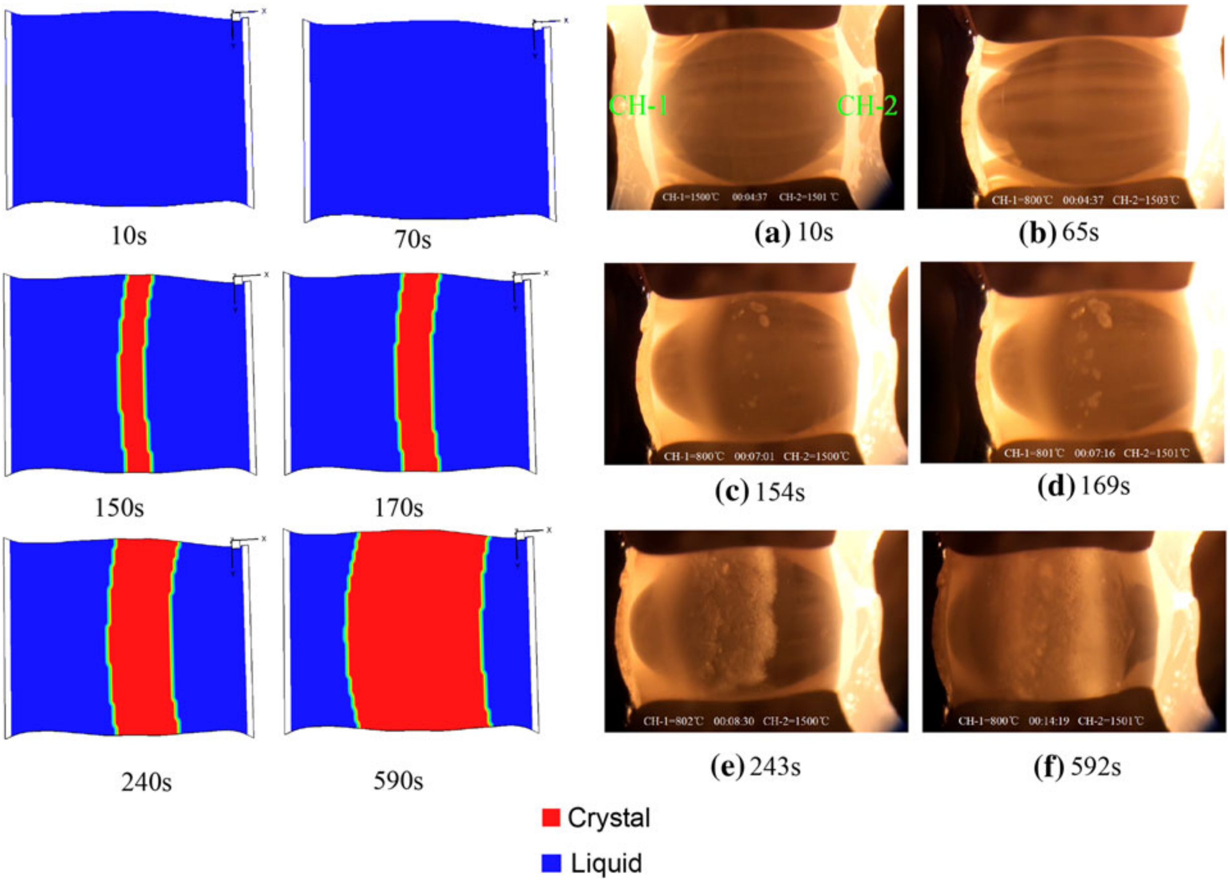

Fig. 22—Comparison of evolving crystallization from model predictions with DHTT experimental observations.

Table AI. Temperature Dependence of Surface Tensions of Pure Components[24]

Oxide	Temperature (K) Dependence of Surface Tension (mN/m)
CaO	$791 - 0.0935T$
SiO_2	$243.2 + 0.031T$
Al_2O_3	$1024 - 0.177T$
MgO	$1770 - 0.636T$
Na_2O/Li_2O	$438 - 0.116T$
CaF_2	$1604.4 - 0.72T$

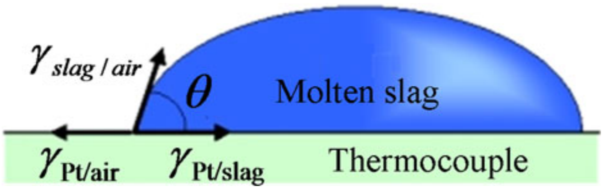

Fig. A1—Young's equation.

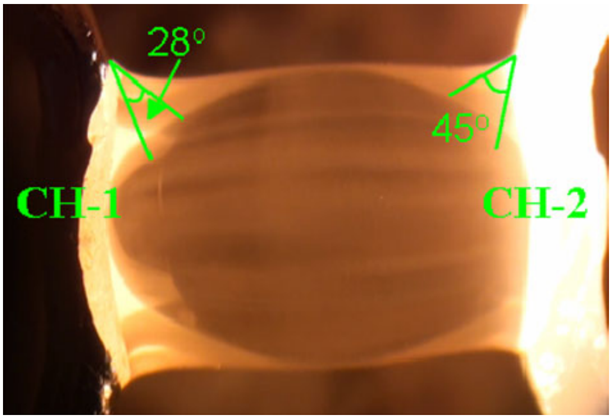

Fig. A2—Contact angles between mold slag and thermocouples.

growth agrees reasonably well with the DHTT experiment measurements.

VI. CONCLUSIONS AND FUTURE WORK

A three-dimensional numerical model has been developed to simulate the process of mold slag crystallization in the DHTT experiment. This model includes heat transfer, fluid flow, and isothermal crystallization based on a JMA model of measurements in the corresponding SHTT experiment. The model predictions match well with many observations of the experiments. The simulation results identify the importance of non-uniform temperature distribution in these experiments and fluid flow and crystal transport due to Marangoni forces and natural convection. Specific conclusions are summarized as follows:

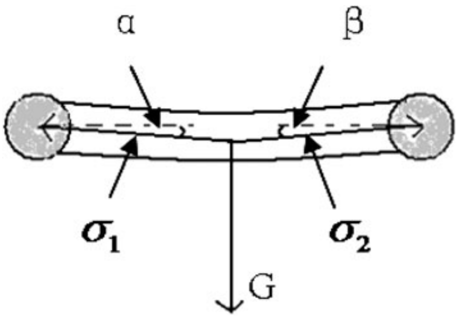

Fig. A3—Force analysis of mold slag.

(1) During the preheating stage 1, although both thermocouples were kept at the same temperature, and the small sample has a very fast (<0.1 second) thermal response, the temperature distribution in the mold slag was non-uniform; temperature in the middle of the mold slag drops significantly, to ~350 K (~77 °C) lower than both thermocouples. This non-isothermal behavior complicates the correct extraction of TTT curves from the experimental measurements.

(2) During the quenching stage 2, the curved temperature profile decreases with the cooling thermocouple. The cooling rate is the greatest at the cold thermocouple (like mold wall) and decreases to zero at the hot thermocouple (like steel shell).

(3) During the holding stage 3, crystallization of the central layer introduces a higher thermal resistance in the middle of the mold flux, which slightly lowers heat flux across the sample, creates nonlinear temperature gradients, and makes the hotter half hotter and the cooler half cooler.

(4) Fluid flows from the hotter region to the cooler region along the surface of the mold slag sample and then recirculates back from the cooler region to the hotter region through the interior, driven by Marangoni flow and natural convection. Slag velocities reach 7 mm/s. This explains the observed movement of crystalline aggregations in molten slag in the small lump-shaped DHTT sample, which is dominated by surface effects. This behavior in the experiment differs from the commercial continuous casting process, where the slag is a thin sheet and fluid flow is driven mainly by other forces such as mold oscillation and shell withdrawal.

(5) The crystallization model correctly predicts the time of onset of crystal formation in the middle of the mold slag sample and growth of the crystallized layer toward both thermocouples.

Considering that thermal fluid flow affects the crystallization of the mold slag and crystallization in turn affects fluid flow, conduction, and radiation, these coupled interactions should be incorporated in future models to enable more accurate predictions.

ACKNOWLEDGMENTS

The authors wish to thank the National Science Foundation of China (51274244), China Scholarship Council, and the Continuous Casting Consortium at the University of Illinois at Urbana-Champaign for support of this project.

APPENDIX: SURFACE TENSION FORCE BALANCE TO FIND SAMPLE SHAPE

Most of the geometry profile of the mold slag in the DHTT experiment can be determined from the top view snapshot from the recorded video, as shown in Figure 3(a). However, the possible deformation (sagging) of the mold slag sample due to gravity cannot be observed directly. This deformation is instead calculated by a force balance.

The surface tension of the mold slag was estimated using a partial molar approach[25]:

$$\gamma_{\mathrm{slag/air}} = \sum x_{\mathrm{i}}\gamma_{\mathrm{i}} = 624.36 - 0.12T \qquad [\mathrm{A1}]$$

where $\gamma_{\mathrm{slag/air}}$ is the surface tension of the mold slag, X_{i} is mole fraction of each pure mineral component in the flux from Table I, and γ_{i} is the temperature-dependent surface tension of each molten mineral, given in Table AI.[24] From Eq. [A1], the surface tension gradient can be calculated as −0.00012 N/m/K.

The surface tension of the type B thermocouple in air was taken to be that of Pt as follows[26]:

$$\gamma_{\mathrm{Pt/air}} = 1746 - 0.307\,[T - 2043\ \mathrm{K}\ (1770\ ^{\circ}\mathrm{C})] \qquad [\mathrm{A2}]$$

Hence, according to Young's Eq. [A3],

$$\gamma_{\mathrm{Pt/slag}} = \gamma_{\mathrm{Pt/air}} - \gamma_{\mathrm{slag/air}}\cos\theta \qquad [\mathrm{A3}]$$

where $\gamma_{\mathrm{Pt/slag}}$ is interface tension between the thermocouple and molten slag and θ is contact angle between the thermocouple and molten slag.

Those contact angles were measured directly from the experimental video screenshot as shown in Figure A2.

Left thermocouple (CH-1): contact angle at $T_1 = 1073$ K (800 °C) is $\theta_1 = 28$ deg.
Right thermocouple (CH-2): contact angle at $T_2 = 1773$ K (1500 °C) is $\theta_2 = 45$ deg.

Therefore, adding the temperature $T_1 = 1073$ K (800 °C) and $T_2 = 1773$ K (1500 °C) into Eq. [A3], the mold slag surface tensions at CH-1 and CH-2 are $\gamma^{1}_{\mathrm{Pt/slag}} = 1606.14$ mN/m and $\gamma^{2}_{\mathrm{Pt/slag}} = 1537.73$ mN/m , respectively.

To find the geometry of the mold slag after deforming due to gravity, the angles α and β, which are the deviation angles from the horizon line as shown in Figure A3, are obtained by the force balance pictured in Figure A3.

The gravity force G is calculated as follows:

$$G = mg = \rho V g = 4.61 \times 10^{-5}\ \mathrm{N} \qquad [\mathrm{A4}]$$

where m is mass, g is gravity acceleration 9.8 m/s^2, ρ is density (2550 kg/m^3 was chosen here), and V is volume of the mold slag sample $2.5 \times 2.17 \times 0.34$ mm^3.

The interfacial adhesive forces between the mold slag and thermocouples are

$$\sigma_1 = \gamma^{1}_{\mathrm{Pt/slag}} \times L_1 \qquad [\mathrm{A5}]$$

$$\sigma_2 = \gamma^{2}_{\mathrm{Pt/slag}} \times L_2 \qquad [\mathrm{A6}]$$

where L_1 and L_2 are the contact lines between the slag and thermocouples and $L_1 = L_2 = 2.17 + 0.34 + 0.34 + 2.17 = 5.02$ mm.

Hence, $\sigma_1 = 8.06 \times 10^{-3}$ N, $\sigma_2 = 7.72 \times 10^{-3}$ N.

From Figure A3, the force balance equations are

$$\sigma_1 \times \cos\alpha = \sigma_2 \times \cos\beta \qquad [\mathrm{A7}]$$

$$\sigma_1 \times \sin\alpha + \sigma_2 \times \sin\beta = G \qquad [\mathrm{A8}]$$

So, $\alpha \cong \beta = 0.17$ deg.

Therefore, with small angles α and β, the deformation (sagging) of the mold slag sample due to gravity is also very small and could be ignored in this study. The final geometry is shown in Figure 5.

REFERENCES

1. K.C. Mills, A.B. Fox, Z. Li, and R.P. Thackray: *Ironmaking Steelmaking*, 2005, vol. 32 (1), pp. 26–34.
2. Y. Meng, B.G. Thomas, A.A. Polycarpou, H. Henein, and A. Prasad: *MS & T 2004 Conference Proceeding*, New Orlean, LA, AIST, Warrendale, PA, 2004, pp. 57–67.
3. Y. Kashiwaya, C.E. Cicutti, A.W. Cramb, and K. Ishii: *ISIJ Int.*, 1998, vol. 38 (4), pp. 348–56.
4. Y. Kashiwaya, C.E. Ciutti, and A.W. Cramb: *ISIJ Int.*, 1998, vol. 38 (4), pp. 357–65.
5. H. Nakada and K. Nagata: *ISIJ Int.*, 2006, vol. 46 (3), pp. 441–49.
6. J.W. Cho and S.Y. Kim: *J. Korean Inst. Met. Mater.*, 2004, vol. 42 (3), pp. 302–03.
7. A.W. Cramb: *Report: American Iron and Steel Institute, Technology Roadmap Program*, Pittsburgh, PA, 2003.
8. G. Wen, H. Liu, and P. Tang: *J. Iron. Steel Res. Int.*, 2008, vol. 15 (4), pp. 32–37.
9. J.L. Klug, R. Hagemann, N.C. Heck, A.C.F. Vilela, and H.P. Heller: *Technol. Metal. Mater. Miner. São Paulo*, 2012, vol. 9 (1), pp. 30–36.
10. N. Kölbl, I. Marschall, and H. Harmuth: *J. Mater. Sci.*, 2011, vol. 46 (19), pp. 6248–54.
11. ANSYS, Inc.: *ANSYS FLUENT 13.0 Getting Started Guide*, Published, 2010.
12. L. Zhou, W. Wang, D. Huang, J. Wei, and J. Li: *Metall. Mater. Trans. B*, 2012, vol. 43B, pp. 925–36.
13. ANSYS, Inc.: *ANSYS FLUENT 13.0 Theory Guide*, Published in the U.S.A., 2010.
14. N.X. Sun, X.D. Liu, and K. Lu: *Scripta Mater.*, 1996, vol. 34, pp. 1201–07.
15. L. Zhou, W. Wang, F. Ma, J. Li, J. Wei, H. Matsuura F. Tsuhihashi: *Metall. Mater. Trans. B*, 2012, vol. 43B, pp. 354–62.

16. Y. Meng and B.G. Thomas: *Metall. Mater. Trans. B*, 2003, vol. 34B, pp. 707–25.
17. J.A. Dantzig and C.L. Tucker: *Modeling in Materials Processing*, Cambridge University Press, New York, 2001.
18. Y. Meng and B.G. Thomas: *ISIJ Int.*, 2006, vol. 45 (5), pp. 660–69.
19. K.C. Mills, A.B. Fox, R.P. Thackray, and Z. Li: *VII International Conference on Molten Slags Fluxes and Salts*, The South African Institute of Mining and Metallurgy, Cape Town, 2004, pp. 713–22.
20. K. Gu, W. Wang, L. Zhou, F. Ma, and D. Huang: *Metall. Mater. Trans. B*, 2012, vol. 43B, pp. 943–55.
21. W. Wang and A.W. Cramb: *ISIJ Int.*, 2005, vol. 45 (12), pp. 1864–70.
22. R.J. O'Malley and J. Neal: *International Conference on New Developments in Metallurgical Process Technology*, Dusseldorf, Germany, 1999, pp. 188–95.
23. H. Nakada, M. Susa, Y. Seko, M. Hayashi, and K. Nagata: *ISIJ Int.*, 2008, vol. 48 (4), pp. 446–53.
24. C. Orrling and A.W. Cramb: *Metall. Mater. Trans. B*, 2000, vol. 31B, pp. 403–06.
25. K. Mills: Short Course as Part of *Southern African Pyrometallurgy*, 2011, pp. 1–49.
26. K.C. Mills and Y.C. Su: *Int. Mater. Rev.*, 2006, vol. 50 (6), pp. 329–51.
27. D. Ye and J. Hu: *Handbook of Thermodynamic Data for Inorganic Materials*, Metallurgical Industry Press, Beijing, 2002.
28. R.M. McDavid and B.G. Thomas: *Metall. Mater. Trans. B*, 1996, vol. 27B, pp. 672–85.
29. V.N. Neelakantan, S. Sridhar, K.C. Mills, and D. Sichen: *Scand. J. Metall.*, 2002, vol. 31 (3), pp. 191–200.
30. Y. Meng and B.G. Thomas: *Metall. Mater. Trans. B*, 2003, vol. 34B, pp. 685–705.
31. K.C. Mills and S. Sridhar: *Ironmaking Steelmaking*, 1999, vol. 26 (4), pp. 262–68.
32. S.A. Nelson and I.S.E. Carmichael: *Contributions Mineral. Petrol.*, 1979, vol. 71, pp. 117–24.
33. C. Robelin and P. Chartrand: *Metall. Mater. Trans. B*, 2007, vol. 38B, pp. 881–92.
34. M. Hanao, T. Tanaka, M. Kawamoto, and K. Takatani: *ISIJ Int.*, 2007, vol. 47 (7), pp. 935–39.